HHS Public Access

Author manuscript

*Proc SPIE Int Soc Opt Eng*. Author manuscript; available in PMC 2017 November 28.

Published in final edited form as:

*Proc SPIE Int Soc Opt Eng*. 2015 ; 9417: . doi:10.1117/12.2082059.

# Characterizing Trabecular Bone structure for Assessing Vertebral Fracture Risk on Volumetric Quantitative Computed Tomography

**Mahesh B. Nagarajan**[1], **Walter A. Checefsky**[1], **Anas Z. Abidin**[1], **Halley Tsai**[1], **Xixi Wang**[1], **Susan K. Hobbs**[1], **Jan S. Bauer**[3], **Thomas Baum**[3], and **Axel Wismüller**[1,2]

[1]Departments of Imaging Sciences and Biomedical Engineering, University of Rochester, New York, United States

[2]Institute for Clinical Radiology, Ludwig Maximilian University, Munich, Germany

[3]Institute for Diagnostic Radiology, Technical University of Munich, Munich, Germany

## Abstract

While the proximal femur is preferred for measuring bone mineral density (BMD) in fracture risk estimation, the introduction of volumetric quantitative computed tomography has revealed stronger associations between BMD and spinal fracture status. In this study, we propose to capture properties of trabecular bone structure in spinal vertebrae with advanced second-order statistical features for purposes of fracture risk assessment. For this purpose, axial multi-detector CT (MDCT) images were acquired from 28 spinal vertebrae specimens using a whole-body 256-row CT scanner with a dedicated calibration phantom. A semi-automated method was used to annotate the trabecular compartment in the central vertebral slice with a circular region of interest (ROI) to exclude cortical bone; pixels within were converted to values indicative of BMD. Six second-order statistical features derived from gray-level co-occurrence matrices (GLCM) and the mean BMD within the ROI were then extracted and used in conjunction with a generalized radial basis functions (GRBF) neural network to predict the failure load of the specimens; true failure load was measured through biomechanical testing. Prediction performance was evaluated with a root-mean-square error (RMSE) metric. The best prediction performance was observed with GLCM feature 'correlation' (RMSE = 1.02 ± 0.18), which significantly outperformed all other GLCM features ($p < 0.01$). GLCM feature correlation also significantly outperformed MDCT-measured mean BMD (RMSE = 1.11 ± 0.17) ($p < 10^{-4}$). These results suggest that biomechanical strength prediction in spinal vertebrae can be significantly improved through characterization of trabecular bone structure with GLCM-derived texture features.

### Keywords

Spinal vertebrae; trabecular bone; biomechanical strength prediction; multi-detector computed tomography; bone mineral density; Minkowski Functionals; support vector regression

[1] mahesh.nagarajan@rochester.edu; phone 585-276-4776; University of Rochester, NY.

This work is not being and has not been submitted for publication or presentation elsewhere.

## 1. MOTIVATION/PURPOSE

Osteoporosis is one of the most common age-related diseases among elderly people and is usually characterized by imbalances in bone resorption and apposition resulting in bone density deterioration. The progression of osteoporosis can lead to osteoporotic fractures, which reduces the quality of life and increases the mortality rate. This highlights the need for accurate fracture risk estimation for clinical evaluation and management of osteoporosis.

Dual-energy X-ray absorptiometry (DXA) is currently the standard technique for bone quality evaluation in terms of bone mineral density (BMD) for purposes of assessing fracture risk [1–2]. Recently, quantitative computer tomography (QCT) has been introduced for extracting BMD measurements exclusively from the trabecular compartment while overcoming certain shortcomings of DXA [3–5]. However, while BMD has been a key clinical factor for fracture risk estimation, it does not completely account for individual fracture risk since it does not provide a complete description of bone quality. Variations in trabecular bone density and structure are also important factors that affect bone strength, and such a deteriorated bone structure in the trabecular compartment can drastically increase the fracture risk.

We are specifically interested in image features that look beyond the bone density and analyze trabecular bone micro-architecture. One area of focus in this context is the prediction of local bone strength, which is useful for diagnosis and monitoring of osteoporotic bone changes [6]. In this study, we focus on characterization of trabecular bone structure in spinal vertebrae for purposes of fracture risk assessment. While the proximal femur is the preferred site BMD measurements in such analysis, correlations between BMD and spinal fracture status have been previously shown in studies involving volumetric quantitative computed tomography [7]. Here, we use second-order statistical features derived from gray-level co-occurrence matrices (GLCM) for vertebral trabecular bone characterization. Such feature can serve as inputs for subsequent supervised learning algorithms to construct models for bone strength prediction. More importantly, such features to complement BMD measures and predict local bone strength, which can be useful for diagnosis and monitoring of osteoporotic bone changes [6,8–9]. This work is embedded in our group’s endeavor to expedite ‘big data’ analysis in biomedical imaging by means of advanced pattern recognition and machine learning methods for computational radiology, e.g. [10–40].

In this contribution, we present preliminary evidence to suggest that GLCM-derived descriptors of trabecular bone structure, as extracted from MDCT images of spinal vertebrae, can improve upon bone strength prediction achieved by MDCT-derived BMD measurements.

## 2. DATA

### Femur Specimens

The donors had dedicated their body for educational and research purposes to the local Institute of Anatomy prior to death, in compliance with local institutional and legislative

requirements. The study protocol was reviewed and approved by the local Institutional Review Boards. Donors with a history of pathological bone changes other than osteoporosis (i.e., bone metastases, hematological, or metabolic bone disorders) were excluded at the outset. Surrounding muscle and fat tissue was completely removed from the spinal 3-segment units. Then, half of the upper and lower vertebra of the spinal 3-segment units was removed with a band saw to create functional spinal segment units with intact ligaments, inter-vertebral discs, and posterior elements. In case of thoracic segment units, the costo-vertebral joints were kept intact by dissecting the costae distally of the costo-vertebral joints. For the purpose of conservation, all functional spinal segment units were stored in formalin solution during the study and degassed at least 24 h before imaging to prevent air artifacts. The functional spinal segment units were sealed in vacuum plastic bags during imaging.

## Multi-detector Computed Tomography (MDCT)

The MDCT images of the functional spinal segment units were acquired by using a whole-body 256-row CT scanner (iCT, Philips Healthcare, Best, The Netherlands). Scan parameters were a tube voltage of 120 kVp, a tube load of 585 mAs, an image matrix of 1024 × 1024 pixels, and a field of view of 150 mm. Transverse sections were reconstructed with a high-resolution bone kernel (YE). The interpolated voxel size was of 146 × 146 × 300 micrometer$^3$, while the real spatial resolution, as determined at q50 of the modulation-transfer-function, was 250 × 250 × 600 micrometer$^3$. A dedicated calibration phantom (Mindways Osteoporosis Phantom, San Francisco, CA, USA) was placed in the scanner mat beneath the functional spinal segment units.

## Post-processing and Region of Interest (ROI) selection

A semi-automated method was used to place a circular ROI on the central axial slice of the middle vertebrae. This involved manual annotation of the vertebral outline which was subsequently eroded to eliminate cortical bone. An automated algorithm was then used to fit the largest possible circle to capture the trabecular compartment in the ventral portion region of the vertebrae. Special care was taken to avoid inclusion of dorsal portion of the vertebrae where invasion by venous plexus and blood vessels was not uncommon.

## BMD Measurements

Pixel attenuations (Hounsfield units or HU) on MDCT images were converted to values indicative of BMD using a reference Mindaways calibration phantom. This phantom consisted of a plastic base containing 5 rods of reference material with varying densities of water and $K_2HPO_4$, as shown in Figure 1. The measured HU of these 5 rods and their corresponding equivalent water and $K_2HPO_4$ densities are used to estimate slope and intercept parameters, i.e. $\sigma_{CT}$ and $\beta_{CT}$, of a linear model for converting HU values to BMD within a specified ROI. The HU values of these reference phantom rods and their known $K_2HPO_4$ densities (Table 1) are used to construct a linear model, i.e.

$$\rho_{\mathrm{ROI}} \frac{\mu_{\mathrm{ROI}} - \beta_{\mathrm{CT}}}{\sigma_{\mathrm{CT}}},$$

where $\mu_{ROI}$ is the HU at a specific pixel or within a specific ROI, and $\rho_{ROI}$ is the corresponding bone mineral density in terms of equivalent $K_2HPO_4$ density. Examples of ROIs where pixel values have been converted to BMD are shown in Figure 2.

### Biomechanical Tests

The half-dissected upper and lower vertebrae of the functional spinal segment units were embedded in resin (Rencast Isocyanat and Polyol, Huntsman Group, Bad Säckingen, Germany) up to 2 mm above, respectively, below their vertebral endplates. The fixation was performed with parallel alignment of the upper and lower endplate of middle vertebra with the outer surface of the resin chock to guarantee strict axial loading conditions of the middle vertebra during the uniaxial biomechanical test. After embedding, the functional spinal segment units were fixed in a mechanical testing system (Wolpert Werkstoffprüfmaschinen AG, Schaffhausen, Switzerland). Ten pre-conditioning cycles with uniaxial tension–compression up to a load between 10 and 400 N with a rate of 5 mm/min was applied. Then a monotonic, uniaxial compression was performed at the same rate. The load–displacement curve was recorded and vertebral failure load was defined as the first peak of the load–displacement curve with a subsequent drop of >10 %.

## 3. METHODS

### BMD Features

The BMD distribution within the ROI was represented by its mean. This measure of BMD on MDCT has been shown to be highly correlated to conventionally used DXA-derived mean BMD [8].

### GLCM Features

For a certain ROI with number of gray-levels $G$, a matrix of dimensions $G \times G$ can be generated indicating the frequency with which any two specific gray-levels occur at a certain distance $d$ apart in a certain direction. For the 2-D scenario, such a gray-level co-occurrence matrix (GLCM) can be generated in four principal directions i.e. 0°, 45°, 90° and 135°. These frequencies can be normalized to yield the joint probability of gray level values occurring as neighboring pairs. For each directional GLCM, the element at a certain row $i$ and column $j$ indicates the frequency at which gray level values $i$ & $j$ occur as neighboring pairs *in that specific direction*. The non-directional GLCM obtained by summing these directional matrices form the basis for several second-order statistical measures that serve as texture features; these are outlined in [41,42]. We investigated 6 of these features that were the least correlated and most commonly used, i.e., absolute value, contrast, energy, homogeneity, correlation and entropy [43].

### Function Approximation

After the computation of different trabecular bone characterizing features sets, their ability to predict the biomechanical strength of the femur specimens (measured by failure load) was evaluated. For this study, a generalized radial basis function neural network was trained to act as a function approximator [44].

### Prediction Performance

In order to generalize the prediction performance of the image features, the set of VOIs was divided into training and test sets. In one iteration, a randomly selected training set of VOIs (80%) was used to approximate the target function (failure load). The resulting model was used to predict the failure load of the remaining, independent test set. The average residual error between the predicted failure load $FL_{pred}$ and the true failure load $FL_{true}$ for the VOIs in this test set $T_i$, $i = 1,..,N_{iter}$, was measured by the root-mean-square error,

$$\mathrm{RMSE}_{\mathrm{T}_i} \sqrt{\langle(\mathrm{FL}_{\mathrm{pred}} - \mathrm{FL}_{\mathrm{true}})^2\rangle_{\mathrm{T_i}}}.$$

This iteration was repeated $N_{iter} = 50$ times resulting in a RMSE distribution for each bone feature set. A Wilcoxon signed-rank test was used to compare two RMSE distributions and test for statistical significant differences in performance.

The statistical analysis, feature extraction, function approximation, performance evaluation and significance testing were performed in MATLAB, version R2010a (MathWorks, Natick, MA).

## 4. RESULTS

The prediction performances of different features with the GRBF function approximator are shown in Figure 3. The best prediction performance was observed with GLCM feature correlation (RMSE = 1.02 ± 0.18), which significantly outperformed all other GLCM features ($p < 0.01$). GLCM feature correlation also significantly outperformed MDCT-measured mean BMD (RMSE = 1.11 ± 0.17) ($p < 10^{-4}$).

## 5. NEW AND BREAKTHROUGH WORK

BMD measurements, measured through MDCT or DXA, do not account for a complete description of trabecular bone in terms of quality or microstructure. Thus, the accuracy of BMD in predicting bone strength or its subsequent use in osteoporosis diagnosis is limited. We address this shortcoming by pursuing a more complex global characterization of trabecular bone micro-architecture in spinal vertebrae. Specifically, we used GLCM-derived second-order statistical features for characterizing trabecular structure in the vertebral compartment. In addition, where previous studies have investigated the use of multi-regression for predicting failure load, we investigate the use of a sophisticated machine learning algorithm, i.e. a GRBF neural network, to construct the bone strength prediction model. Our results show that such GLCM-derived texture features, when used in combination with neural networks, can contribute to improvements in biomechanical strength prediction, especially when compared to more BMD measurements derived from MDCT.

We are also interested in investigating other novel methods for characterizing trabecular bone micro-architecture in spinal vertebrae through their topology (Minkowski Functionals [45]) or local geometry (scaling index method [46]) in future studies. Such methods could

yield a superior characterization of the bone structures under investigation, or complement those already investigated in this study. One can also quantify the anisotropy of the trabecular bone structure and evaluate its relationship to overall bone strength in the vertebrae.

## 6. CONCLUSION

In conclusion, the results presented in this work indicate that GLCM-derived second-order statistical features that characterize trabecular bone structure in spinal vertebrae can significantly improve the prediction of biomechanical strength when compared to conventional approaches. This could play an important role in bone fracture risk prediction and osteoporosis diagnosis in future computer-aided diagnostic applications.

## Acknowledgments

This research was funded in part by the National Institute of Health (NIH) Award R01-DA-034977, the Harry W. Fischer Award of the University of Rochester, the Clinical and Translational Science Award 5-28527 within the Upstate New York Translational Research Network (UNYTRN) of the Clinical and Translational Science Institute (CTSI), University of Rochester, by the Center for Emerging and Innovative Sciences (CEIS), a NYSTAR-designated Center for Advanced Technology and by the Deutsche Forschungsgemeinschaft (DFG BA 4085/2-1 (to J.S.B.) and BA 4906/1-1 (to T.B.)). The content is solely the responsibility of the authors and does not necessarily represent the official views of the National Institute of Health. This work was conducted as a Practice Quality Improvement (PQI) project related to American Board of Radiology (ABR) Maintenance of Certificate (MOC) for Prof. Dr. Axel Wismüller. Prof. Dr. Dr. Maximilian Reiser, FACR, FRCR of the Department of Radiology, Ludwig Maximilian University Munich, Germany, is also acknowledged for his continued support.

## References

1. Kanis JA, Borgstrom F, De Laet C, Johansson H, Johnell O, Jonsson B, Oden A, Zethraeus N, Pfleger B, Khaltaev N. Assessment of fracture risk. Osteoporosis International. 2005; 16(6):581–589. [PubMed: 15616758]
2. Boehm H, Eckstein F, Wunderer C, Kuhn V, Lochmueller EM, Schreiber K, Mueller D, Rummeny EJ, Link TM. Improved performance of hip DXA using a novel region of interest in the upper part of the femoral neck: in vitro study using bone strength as a standard of reference. Journal of Clinical Densitometry. 2005; 8(4):488–494. [PubMed: 16311437]
3. Lang TF, Keyak JH, Heitz MW, Augat P, Lu Y, Mathur A, Genant HK. Volumetric quantitative computed tomography of the proximal femur: precision and relation to bone strength. Bone. 1997; 21(1):101–108. [PubMed: 9213015]
4. Bousson V, Le Bras A, Roqueplan F, Kang Y, Mitton D, Kolta S, Bergot C, Skalli W, Vicaut E, Kalender W, Engelke K, Laredo JD. Volumetric quantitative computed tomography of the proximal femur: relationships linking geometric and densitometric variables to bone strength role for compact bone. Osteoporosis International. 2006; 17(6):855–864. [PubMed: 16547689]
5. Genant HK, Block JE, Steiger P, Glueer C-C, Smith R. Quantitative computed tomography in assessment of osteoporosis. Seminars in Nuclear Medicine Bone Density Studies. 1987; 17:316–333.
6. Bauer JS, Link TM. Advances in osteoporosis imaging. European Journal of Radiology. 2009; 71(3):440–449. [PubMed: 19651482]
7. Lang TF, Guglielmi G, van Kuijk C, De Serio A, Cammisa M, Genant HK. Measurement of bone mineral density at the spine and proximal femur by volumetric quantitative computed tomography and dual-energy x-ray absorptiometry in elderly women with and without vertebral fractures. Bone. 2002; 30(1):247–250. [PubMed: 11792593]
8. Bauer JS, Kohlmann S, Eckstein F, Mueller D, Lochmüller EM, Link TM. Structural analysis of trabecular bone of the proximal femur using multislice computed tomography: a comparison with

dual x-ray absorptiometry for predicting biomechanical strength in vitro. Calcified Tissue International. 2006; 78(2):78–89. [PubMed: 16467973]

9. Baum T, Carballido-Gamio J, Huber MB, Mueller D, Monetti R, Räth C, Eckstein F, Lochmüller EM, Majumdar S, Rummeny E, Link TM, Bauer JS. Automated 3D trabecular bone structure analysis of the proximal femur prediction of biomechanical strength by CT and DXA. Osteoporosis International. 2010; 21:1553–1564. [PubMed: 19859642]
10. Bunte K, Hammer B, Wismüller A, Biehl M. Adaptive local dissimilarity measures for discriminative dimension reduction of labeled data. Neurocomputing. 2010; 73(7):1074–1092.
11. Wismüller A, Vietze F, Dersch DR. Segmentation with neural networks. Handbook of Medical Imaging. 2000:107–126.
12. Leinsinger, G., Schlossbauer, T., Scherr, M., Lange, O., Reiser, M., Wismüller, A. Eur. Radiol. Vol. 16. Springer-Verlag; 2006. Cluster analysis of signal-intensity time course in dynamic breast MRI: does unsupervised vector quantization help to evaluate small mammographic lesions?; p. 1138-1146.
13. Wismüller A, Vietze F, Behrends J, Meyer-Baese A, Reiser M, Ritter H. Fully automated biomedical image segmentation by self-organized model adaptation. Neural Networks. 2004; 17(8):1327–1344. [PubMed: 15555869]
14. Hoole P, Wismüller A, Leinsinger G, Kroos C, Geumann A, Inoue M. Analysis of tongue configuration in multi-speaker, multi-volume MRI data. Proc. 5th Semin. Speech Prod. Model. Data CREST Work. Model. Speech Prod. Mot. Plan. Articul. Model. 2000:157–160.
15. Wismüller, A. Ph.D. Thesis. Technical University of Munich, Department of Electrical and Computer Engineering; 2006. Exploratory Morphogenesis (XOM): a novel computational framework for self-organization.
16. Wismüller, A., Dersch, DR., Lipinski, B., Hahn, K., Auer, D. [ICANN 98]. Springer; London: 1998. A neural network approach to functional MRI pattern analysis—clustering of time-series by hierarchical vector quantization; p. 857-862.
17. Wismüller A, Vietze F, Dersch DR, Behrends J, Hahn K, Ritter H. The deformable feature map-a novel neurocomputing algorithm for adaptive plasticity in pattern analysis. Neurocomputing. 2002; 48(1):107–139.
18. Behrends, J., Hoole, P., Leinsinger, GL., Tillmann, HG., Hahn, K., Reiser, M., Wismüller, A. [Bildverarbeitung für die Medizin 2003]. Springer; Berlin Heidelberg: 2003. A segmentation and analysis method for MRI data of the human vocal tract; p. 186-190.
19. Wismüller A, Dersch DR. Neural network computation in biomedical research: chances for conceptual cross-fertilization. Theory in Biosciences. 1997; 116(3):229–240.
20. Bunte K, Hammer B, Villmann T, Biehl M, Wismüller A. Exploratory Observation Machine (XOM) with Kullback-Leibler Divergence for Dimensionality Reduction and Visualization. ESANN. 2010; 10:87–92.
21. Wismüller, A., Vietze, F., Dersch, DR., Hahn, K., Ritter, H. [ICANN 98]. Springer; London: 1998. The deformable feature map—adaptive plasticity for function approximation; p. 123-128.
22. Wismüller, A. [Advances in Self-Organizing Maps]. Springer; Berlin Heidelberg: 2009. The exploration machine--a novel method for data visualization; p. 344-352.
23. Meyer-Bäse, A., Jancke, K., Wismüller, A., Foo, S., Martinetz, T. Eng. Appl. Artif. Intell. Vol. 18. Elsevier; 2005. Medical image compression using topology-preserving neural networks; p. 383-392.
24. Huber, MB., Nagarajan, M., Leinsinger, G., Ray, LA., Wismüller, A. SPIE Med. Imaging. Vol. 7624. International Society for Optics and Photonics; 2010. Classification of interstitial lung disease patterns with topological texture features; p. 762410
25. Wismüller A. The exploration machine: a novel method for analyzing high-dimensional data in computer-aided diagnosis. SPIE Med. Imaging. 2009:72600G – 72600G.
26. Bunte K, Hammer B, Villmann T, Biehl M, Wismüller A. Neighbor embedding XOM for dimension reduction and visualization. Neurocomputing. 2011; 74(9):1340–1350.
27. Wismüller, A. [Advances in Self-Organizing Maps]. Springer; Berlin Heidelberg: 2009. A computational framework for nonlinear dimensionality reduction and clustering; p. 334-343.

28. Huber, MB., Nagarajan, MB., Leinsinger, G., Eibel, R., Ray, LA., Wismüller, A. Med. Phys. Vol. 38. American Association of Physicists in Medicine; 2011. Performance of topological texture features to classify fibrotic interstitial lung disease patterns; p. 2035-2044.
29. Wismüller A, Verleysen M, Aupetit M, Lee JA. Recent Advances in Nonlinear Dimensionality Reduction, Manifold and Topological Learning. ESANN. 2010
30. Wismüller, A., Meyer-Baese, A., Lange, O., Reiser, MF., Leinsinger, G. Med. Imaging, IEEE Trans. Vol. 25. IEEE; 2006. Cluster analysis of dynamic cerebral contrast-enhanced perfusion MRI time-series; p. 62-73.
31. Twellmann, T., Saalbach, A., Müller, C., Nattkemper, TW., Wismüller, A. Detection of suspicious lesions in dynamic contrast enhanced MRI data. Eng. Med. Biol. Soc; IEMBS'04. 26th Annu. Int. Conf. IEEE; 2004. p. 454-457.2004
32. Schlossbauer, T., Leinsinger, G., Wismüller, A., Lange, O., Scherr, M., Meyer-Baese, A., Reiser, M. Invest. Radiol. Vol. 43. NIH Public Access; 2008. Classification of small contrast enhancing breast lesions in dynamic magnetic resonance imaging using a combination of morphological criteria and dynamic analysis based on unsupervised vector-quantization; p. 56
33. Otto TD, Meyer-Baese A, Hurdal M, Sumners D, Auer D, Wismüller A. Model-free functional MRI analysis using cluster-based methods. AeroSense. 2003; 2003:17–24.
34. Varini, C., Nattkemper, TW., Degenhard, A., Wismüller, A. Breast MRI data analysis by LLE. Neural Networks; Proceedings. 2004 IEEE Int. Jt. Conf; 2004. p. 2449-2454.2004
35. Huber, MB., Lancianese, SL., Nagarajan, MB., Ikpot, IZ., Lerner, AL., Wismüller, A. Biomed. Eng. IEEE Trans. Vol. 58. IEEE; 2011. Prediction of biomechanical properties of trabecular bone in MR images with geometric features and support vector regression; p. 1820-1826.
36. Meyer-Base, A., Pilyugin, SS., Wismüller, A. Stability analysis of a self-organizing neural network with feedforward and feedback dynamics. Neural Networks; Proceedings. 2004 IEEE Int. Jt. Conf; 2004. p. 1505-1509.2004
37. Schlossbauer, T., Kallergi, M., Reiser, MF., Wismüller, A., Meyer-Base, A., Lange, O., Leinsinger, G. J. Electron. Imaging. Vol. 15. International Society for Optics and Photonics; 2006. Segmentation and classification of dynamic breast magnetic resonance image data; p. 13020
38. Nagarajan, MB., Huber, MB., Schlossbauer, T., Leinsinger, G., Krol, A., Wismüller, A. Mach. Vis. Appl. Vol. 24. Springer; Berlin Heidelberg: 2013. Classification of small lesions in dynamic breast MRI: eliminating the need for precise lesion segmentation through spatio-temporal analysis of contrast enhancement; p. 1371-1381.
39. Nagarajan, MB., Huber, MB., Schlossbauer, T., Leinsinger, G., Krol, A., Wismüller, A. J. Med. Biol. Eng. Vol. 33. NIH Public Access; 2013. Classification of Small Lesions in Breast MRI: Evaluating The Role of Dynamically Extracted Texture Features Through Feature Selection.
40. Wismüller, A., Meyer-Bäse, A., Lange, O., Auer, D., Reiser, MF., Sumners, D. J. Biomed. Inform. Vol. 37. Academic Press; 2004. Model-free functional MRI analysis based on unsupervised clustering; p. 10-18.
41. Haralick RM, Shanmuga K, Dinstein I. Textural Features for Image Classification. IEEE Transactions on Systems Man and Cybernetics Smc. 1973; 3(6):610–621.
42. Haralick RM. Statistical and Structural Approaches to Texture. Proceedings of the IEEE. 1979; 67(5):786–804.
43. Anys H, He D. Evaluation of textural and multipolarization radar features for crop classification. IEEE Transactions on Geoscience and Remote Sensing. 1995; 33(5):1170–1181.
44. Moody J, Darken CJ. Fast Learning in Networks of Locally-Tuned Processing Units. Neural Computation. 1989; 1:281–294.
45. Michielsen K, Raedt HD. Integral-geometry morphological image analysis. Physics Reports. 2001; 347(6):461–538.
46. Jamitzky F, Stark W, Bunk W, Thalhammer S, Raeth C, Aschenbrenner T, Morfill G, Heckl W. Scaling-index method as an image processing tool in scanning-probe microscopy. Ultramicroscopy. 2000; 86:241–246.

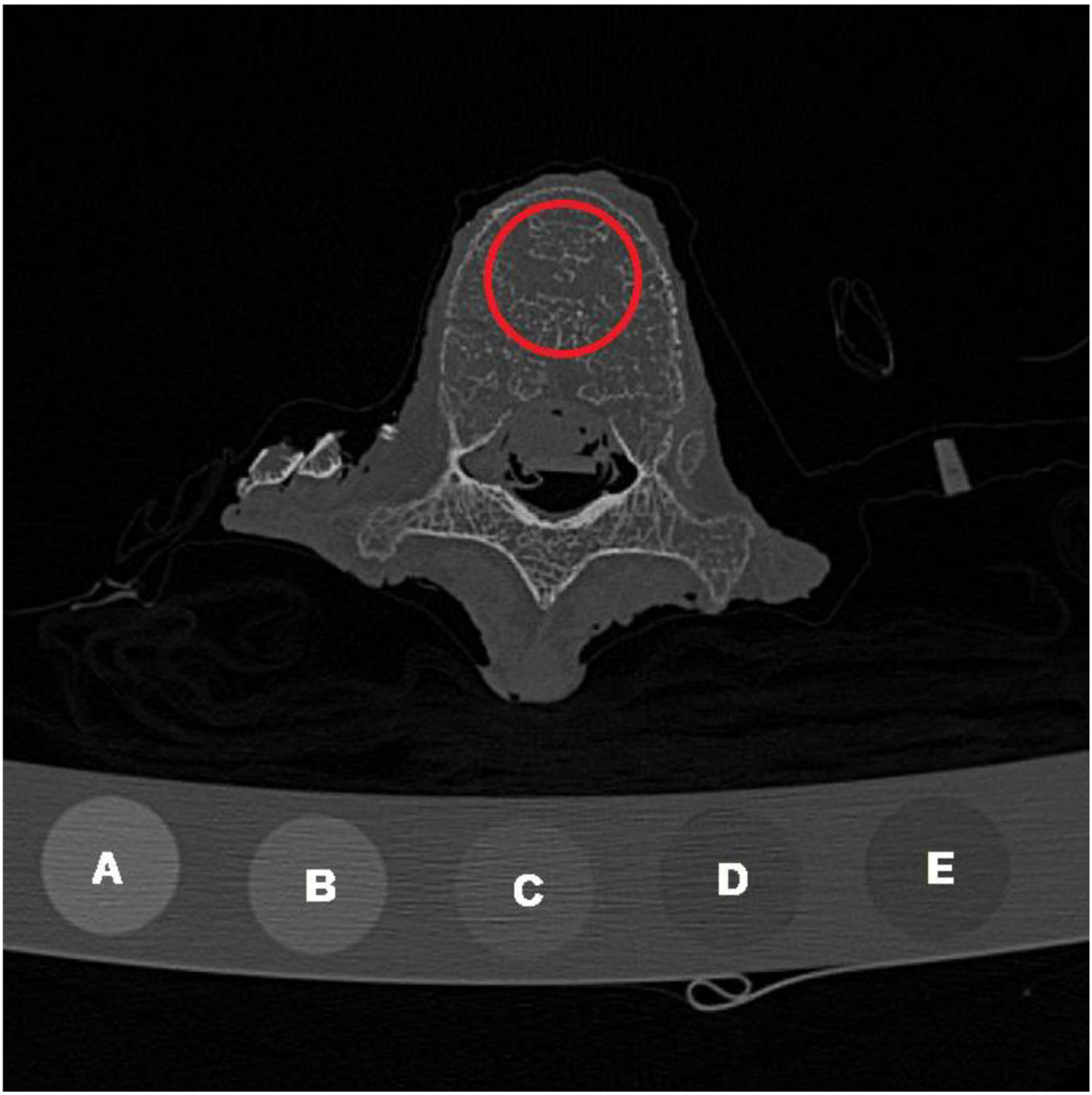


**Figure 1.**
The central axial slice from the middle vertebra. The calibration phantoms A-E are see on the bottom; their equivalent $H_20$ and $K_2HPO_4$ densities are specified in Table 1. The ROI selected for analysis of trabecular bone structure is marked in red.

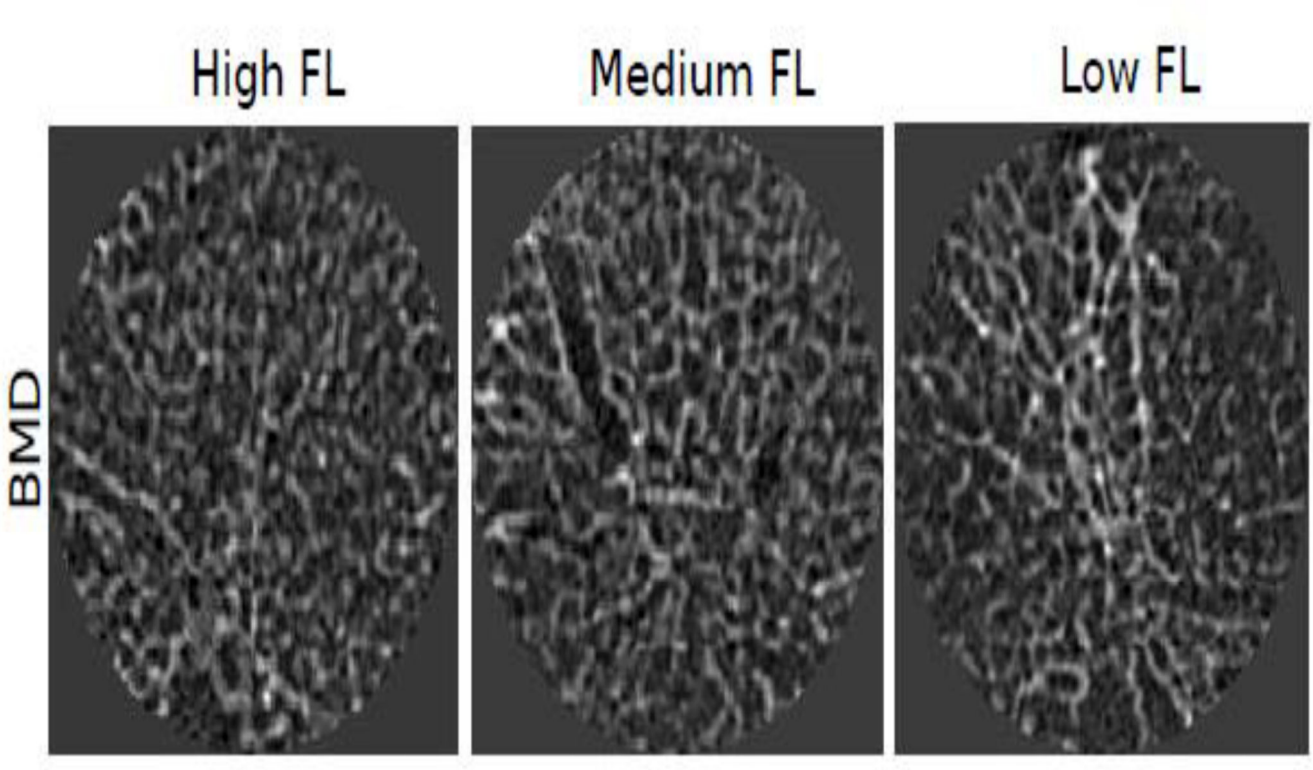


**Figure 2.**
ROIs extracted from the central slice of spinal vertebrae on MDCT and transformed to BMD from HU. From left to righ, ROIs were extracted from specimens that exhibited high, medium and low failure load.

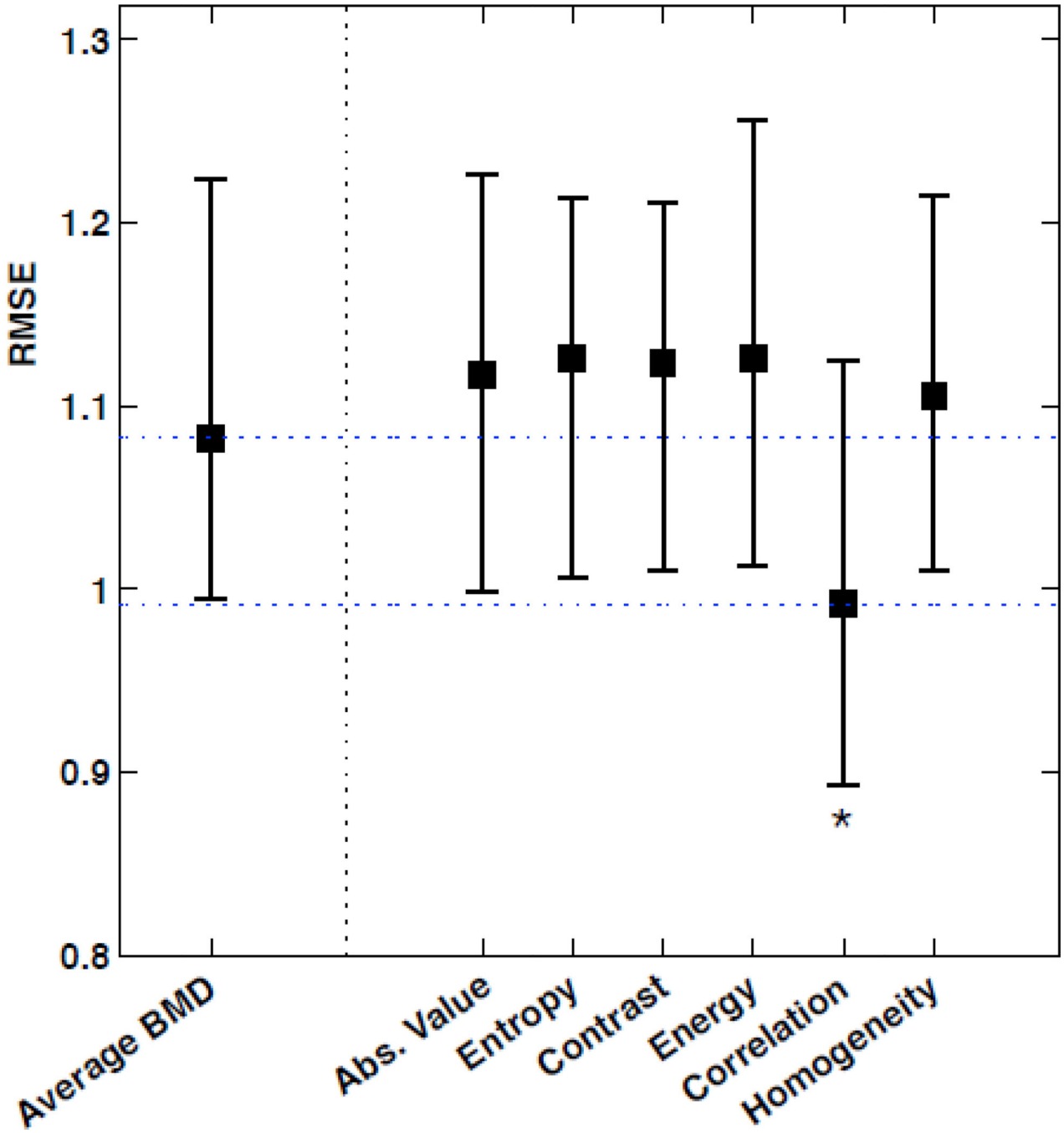


**Figure 3.**

Comparison of prediction performance (mean RMSE ± std) between mean BMD and GLCM features. For each RMSE distribution, the central mark corresponds to the median and the edges are the 25th and 75th percentile. As seen here, the best performance is achieved with GLCM feature correlation.

**Table 1**

Calibration phantom with 5 rods A-E. Actual densities and associated uncertainties determined for the reference materials are shown here.

| Reference | Eq. $H_20$ density (mg/cc) | Eq. K2HPO4 density (mg/cc) |
|---|---|---|
| A | 1012.2 ± 2.3 | −51.8 ± 0.1 |
| B | 1057.0 ± 1.9 | −53.4 ± 0.1 |
| C | 1103.6 ± 1.7 | 58.9 ± 0.1 |
| D | 1119.5 ± 1.8 | 157.0 ± 0.3 |
| E | 923.2 ± 2.1 | 375.8 ± 0.9 |